Hindawi
International Journal of Polymer Science
Volume 2022, Article ID 8038386, 17 pages
https://doi.org/10.1155/2022/8038386

Research Article

Effects of Graphene Oxide and Reduced Graphene Oxide on the Mechanical and Dielectric Properties of Acrylonitrile-Butadiene Rubber and Ethylene-Propylene-Diene-Monomer Blend

Bismark Mensah, David Sasu Konadu, and Benjamin Agyei-Tuffour

Department of Materials Science and Engineering, School of Engineering Sciences, College of Basic and Applied Sciences, University of Ghana, Legon, Accra, Ghana

Correspondence should be addressed to Bismark Mensah; bismarkmensah@ug.edu.gh

Received 13 April 2022; Revised 9 June 2022; Accepted 13 June 2022; Published 29 June 2022

Academic Editor: Hossein Roghani-Mamaqani

The composites of properties of ethylene-propylene-diene-monomer (E) and acrylonitrile butadiene-rubber (N) composites of graphene oxide (GO) and reduced graphene oxide (G) were prepared by a combination of solution and open-roll method. They include single matrices (EGO and EG) and blends N/E, 20 part of hundreds of rubber (phr)/80 phr (A), 80 phr/20 phr (B), and 50 phr/50 phr(C) blend containing GO and G. The physico-mechanical properties including vulcanization, tensile, glass transition temperature (T_g), and dielectric spectroscopic properties were evaluated. The N-rich systems reinforced with GO, cured faster than the E-rich systems. Also, N-rich systems obtained the highest dielectric constant (ε'), especially when GO and G were incorporated, for example, NG and N-GO obtained 317 and 283% increment in ε' than EG and EGO, respectively. In terms of tensile properties, AGO exhibited the highest strength and elongation at break properties (%). Therefore, solution mixing technique of rubber blends filled with nanoinclusion can be achieved with the tendency of reducing cost without the use of compatibilizer and still maintain the integrity of the physical properties of the final product. The result obtained therefore shows that the current compositions can find various applications in oil/gas sealants, heat-resistant applications, and energy storage materials with minimal losses.

1. Introduction

Polymer nanomaterials have found enormous patronage recently in the technology industry due to their lightweight (energy saving capabilities), versatility, and cost effectiveness [1–4]. Elastomers especially possess unique viscoelastic properties, which make them recoverable from deformation upon removal of load [5–9]. When elastomers are crosslinked with fillers, there are significant improvements in their mechanical properties. Prior studies show that fillers or reinforcements such as fibers [10], metal hydroxides [11], nanoclays [12], carbon black (CB) [13], and carbon nanotubes (CNT) [14] result in enhanced physico-mechanical properties that have made them applicable [5–9] in the aerospace/automobile, medical/health, and the electrical/electronic technologies [14–16].

In recent times, complementing elastomers with additives in their desired ratios have observed appreciable enhancement in their properties which could not be attained when single matrices are used [17–21]. However, the miscibility of the elastomers (N/E) is quite challenging and often addressed with the use of compatibilizers and plasticizers. This approach has however not completely resolved the miscibility challenges, even though it is an expensive route, and therefore, alternative methods to improve miscibility in elastomers cannot be undermined. The parameters which influence miscibility of elastomers include mixing time, temperature, methods (melt, solution, or in situ polymerization),

the chemistry, polarity, size, and structure of fillers. The others include quantity and nature of elastomer and chain mobility, and the techniques used are determining the resultant dielectric constant.

Generally, polymers and, especially, elastomer blends have been reported to have inferior dielectric (ε') properties in the order of magnitude of 10 units lower [20, 22–24]. For instance, natural rubber (NR), butyl rubber (BR), NR/E blends, NR/N blends, and SBR have recorded ε' values of ~1–4.82, ~2–3.41, ~2–6.7, ~2–8.63, and~2–5.3, respectively [20]. Reinforcing fillers have been incorporated into polymer matrix to improve the dielectric constants [25, 26]. Example, Razzaghi-Kashani et al. [25] and Lin et al. [11] organically modified SR with montmorillonite (OMMT) and aluminum hydroxide [$(Al(OH)_3$], respectively. Al-Hartomy et al. [27] and Ravikumar et al. [28] recently filled NR with natural graphite (NG) and CB, separately. The results showed that NR-CB showed high ε' compared to NR-NG composites due to the insulating effect of NG. Also, carbon nanotubes have been used in elastomers, and their dielectric properties have been greatly improved according to Mensah et al. [14].

The increased use of graphene and its derivative nanosheets (GDN) in recent times by the rubber-nanotechnology industry stems from the graphene-based reinforcements' high Young's modulus (~1 TPa), strength (~130 GPa), ~5000 W/mK thermal and ~6,000 S/cm electrical conductivities [29–31]. Srinivasarao et al. [32] and Chandran et al. [33] confirmed that reduced graphene oxide (G) showed high ε' compared to rubber-natural graphite (NG) and rubber-CB composites, owing to high electrical conductivity, proper dispersion, and strong bonding of the G with the rubber matrix. Al-Hartomy et al. [27] also confirmed that graphene nanoplatelets exhibited great dielectric performance in NR compared to that of CB. Hence, GDN is used in the form mats and thin coated films on suitable rubber substrates for advanced applications as energy harvesters [34, 35], electromagnetic interference shielding materials [14, 35], rubber contact switches, sensors, electrodes [36–40], and heat sinks [34, 35, 41].

However, a recent study conducted by Chen et al. [42] revealed that even increasing the processing aids; accelerator (steric acid, SA) content actually caused a drop in the dielectric constant whilst increase in the activator zinc oxide (ZnO) and filler content both caused an increase in dielectric constant and the loss factor of NR. These imply that further work is required to address the issues of elastomer-GDN-based dielectric challenges especially with their processing techniques and material design.

In this paper, the effects of GO and G on the N, E, and N/E blends prepared by using a new technique of solution mixing to compound N/E blends in the presence of GO and/or G are presented. This involved open blending by two-roll mills and solution mixing to compound the elastomers with GO and G and cured in a cure rheometer. The crosslinked samples are characterized for their physicomechanical properties including tensile strength, glass transition temperature, and dielectric properties. The implications of the results are discussed to shed more lights on the various techniques used to enhance the dielectric properties of elastomers and their blends.

Table 1: Composition of rubber compounds.

Sample/code	Cure ingredient (phr)∗							
	Rubber	ZnO	CZ	SA	TMTD	S	GO	G
N	100	5	0.5	1.5	0.25	2	—	—
NGO	100	5	0.5	1.5	0.25	2	0.1	—
NG	100	5	0.5	1.5	0.25	2	—	0.1
E	100	5	0.5	1.5	0.25	2	—	—
EGO	100	5	0.5	1.5	0.25	2	0.1	—
EG	100	5	0.5	1.5	0.25	2	—	0.1
A (N/E)	20/80	5	0.5	1.5	0.25	2	—	—
B (N/E)	80/20	5	0.5	1.5	0.25	2	—	—
C (N/E)	50/50	5	0.5	1.5	0.25	2	—	—
AGO	20/80	5	0.5	1.5	0.25	2	0.1	—
BGO	80/20	5	0.5	1.5	0.25	2	0.1	—
CGO	50/50	5	0.5	1.5	0.25	2	0.1	—
AG	20/80	5	0.5	1.5	0.25	2	—	0.1
BG	80/20	5	0.5	1.5	0.25	2	—	0.1
CG	50/50	5	0.5	1.5	0.25	2	—	0.1

(phr)∗: parts per hundred of rubber; CZ: N-cyclohexyl-2-benzothiazolysulfenamide; TMTD: tetramethylthiuram disulfide; S: sulfur; SA: stearic acid; acrylonitrile butadiene rubber (N), ethylene-propylene-diene monomer (E), graphene oxide(GO), and reduced graphene oxide graphene (G).

2. Experimental

2.1. Materials. An acrylonitrile-butadiene rubber (N) under the trade name KNB 25LM™ with acrylonitrile content 20-30% and ethylene-propylene-diene monomer (E) (Vistalon 7500; ethylene content 55.5%, Ethylidene norbornene (ENB) content 5.7%) was supplied by the Kumho Petrochemical Company, Korea. The graphene oxide (GO) was prepared using a modified version of Hummer's method, and the conversion of GO into reduced graphene oxide (G) was achieved by the use of hydrazine. The full detail is reported in our earlier work [43].

The remaining of the curatives, zinc oxide (ZnO), stearic acid (SA), sulfur (S), N-cyclohexile 2-benzotiazole sulfonamide (CZ), and tetramethyl thiuram disulfide (TMTD), were all obtained from Intelligent Polymer Nano Lab (IPNL), Polymer Nanotechnology Department, Jeonbuk National University, South Korea. The compound design expressed as parts per hundred of rubber (phr) with their corresponding codes is presented in Table 1.

2.2. Preparation of Nanocomposites. Table 1 presents the composition and the designation of polar (N), nonpolar (E), their blends (N/E), and their respective composites with GO and G particles. The preparation of the NGO and NG nanocomposite was successfully achieved via solution mixing and open two-roll milling method as detailed in our previous work [43, 44].

Solvent mixing technique was employed to prepare composites made of nonpolar E compounds (E, EGO, and EG), it

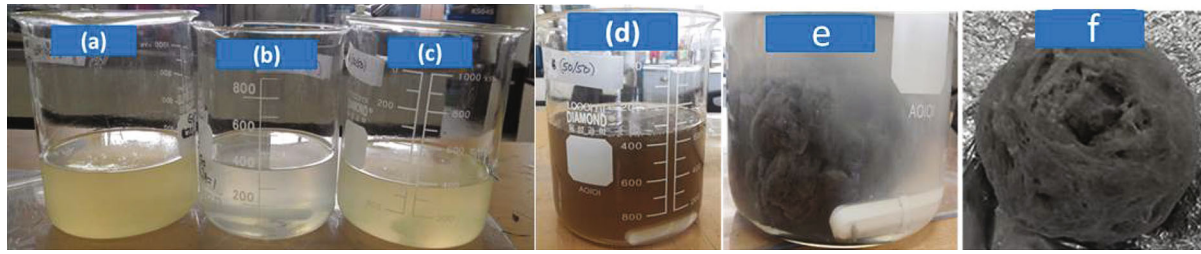

Figure 1: Solution processing of representative samples of N/E blends and their composites with GO and G; (a) 80/20, (b) 20/80, (c) 50/50, (d) 50/50-G solution, (e) coagulation of 50/50-G, and (f) 50/50-G nanocomposite after drying.

was blended with N (A, B, and C) and their respective composites (AGO, BGO, CGO, AG, BG, and CG). Typically, the N/E were cut into pieces and dissolved in toluene under 60°C temperature for ~12 h as shown in Figures 1(a)–1(c). The GO and G were also dispersed in toluene via prolonged ultrasonication for ~2 h, and their size range measured by transmission electron microscopy (TEM) was about ~0.5–5 nm. The GO/toluene and G/toluene solutions were separately mixed with N/E/toluene mixture. The mixture was stirred vigorously on a magnetic stirrer at 60°C for ~12 h until a homogenous phase was formed in Figure 1(d) (50/50-G formulation). Instead of using deionized water as was used previously for only polar matrix (N) in our work [43, 44], an acetone was gradually added to these mixtures while still stirring with a spatula to avoid phase separation between the matrix and graphene sheets. This resulted in coagulation of the composites (50/50-G composite) as shown in Figure 1(e). The resulting compound was oven dried at 80°C until the weight of the solid mass was recovered as shown in Figure 1(f).The curing additives (ZnO, TMTD, SA, CZ, and S) were gradually added and mixed to obtain solid masses of filled and unfilled compounds by using a two-roll mill (Farrel 8422, USA). The rubber compounds were sheeted out and left overnight. About 9~10 g of each sample was cut and cured by a cure rheometer to determine the optimum cure time. The cure time was used to vulcanize the various compositions by using a square mold of dimension (15 cm × 15 cm) and ~0.1 cm thickness with a hot press machine (Caver WMV50H, USA). The hot press conditions included a pressure of ~11 MPa and at 160°C. The cured samples were left overnight to cool and afterwards cut into standard shapes for further characterizations.

2.3. Synthesis and Characterization of GO and G-Sheets. A solution of GO/dimethyl furan (DMF) and G-sheets/DMF was prepared by prolonged sonication for ~1 h. The solutions were separately dropped gently on TEM 200-mesh of copper grids and were allowed to dry. TEM images of the physical structures of GO and G-sheets were observed with transmission electron microscope (TEM, JEOL, and JEM2100). Fourier transform infrared (FTIR) spectra of the GO and G-sheets were recorded on a Jasco FTIR-4200 spectrophotometer (USA).

In the dynamic light scattering analysis, 20 mg of GO and G-sheets was, respectively, weighed into a falcon tube and 40 ml of distilled water (DW) added and sonicated for 30 minutes at room temperature. Afterwards, the GO and G-sheets were dispersed completely in DW and probe sonicated (power = 450 W, frequency = 20 kHz) for 4 hat ~40% amplitude each. The temperature of the G and GO solutions was maintained using an ice bath during sonication. Then, the probe sonicated mixture was centrifuged at 12000 rpm severally until no precipitate settled down. The average sheet sizes for the solution were observed within 90-113 nm using the DLS machine (Jeonbuk National University (JBNU)).

The structure of the G and GO was determined using X-PERT X-ray diffractometer (PANalytical X-PERT Powder diffractometer) with Cu-Kα radiation (40 kV, 100 mA, λ = 0.154 nm). The X-ray diffraction patterns were obtained at room temperature with a scan step of 0.016711 (continuous type). The d-spacing of the particles was calculated using the Bragg's equation.

2.4. Characterization of Graphene-Elastomer Composites. The curing properties of GO, G fillers-N, E, and N/E composites were studied using an oscillating-die rheometer (MDR, model: PDR2030, TESTONE. Ltd., South Korea) operating at 160°C. The curing parameters including maximum (M_H), minimum (M_L), change in torque (ΔM), onset of cure time (t_{s2}), optimum cure time (t_{90}), and curing rate index (CRI = $100/(t_{90} - t_{s2})$) of the composites were extracted from the rheo-curves, analyzed, and were presented. FTIR spectra of the composites were again determined using the Jasco FTIR-4200 spectrophotometer (USA).

The tensile properties of GO, G–elastomers composites were determined according to ASTM D412 standard using the universal tensile machine (UTM, LLOYD machine, UK) with dumbbell-shaped specimen. The specimen was subjected to stress-strain test at a crosshead speed of ~500 mm/min at room temperature. The tensile properties, elongation at break, E_{br} (%), and the ultimate tensile strength, UTS (MPa), were deduced from the stress-strain curve. The procedure was repeated for at least four (4) composite samples, and the average results were reported.

2.4.1. Dielectric Spectroscopy Study. The dielectric constant (ε') of the N, E, and N/E reinforced with GO and G was measured by using an LCR meter (VHR-200, USA). The frequency range selected was 1 ~10^6 Hz, with steps of 1 Hz and a voltage of ~0.5 v. The sample was coated (top and bottom) with silver grease electrode to reduce the surface resistance of the samples. This was for good electrical

connection between the samples and the electrodes. The frequency of silver grease electrode coatings was maintained and was carefully monitored and controlled to ensure that a uniform sample thickness was achieved. The samples were then connected to the applied field using a copper tape. The average sample dimension was $\sim 2 \times 2$ cm and ~1 mm thick. All the measurements were carried out at room temperature.

Given that the real part of the complex dielectric constant is shown in

$$\varepsilon* = \varepsilon' + i\varepsilon'', \tag{1}$$

where the ε' and loss tangent ($\tan\delta$) were, respectively, calculated using the relationships in Equations (2) and (3) as follows:

$$\varepsilon' = \frac{Ct}{A\varepsilon_o}, \tag{2}$$

$$\tan\delta = \frac{\varepsilon''}{\varepsilon'}, \tag{3}$$

where ε' is the real part of dielectric constant, ε'' is the dielectric loss modulus, C is the capacitance, t is the thickness of the samples (~0.1 cm), ε_o is the permittivity in vacuum (8.85×10^{-15}F/cm), and A is the coated area of the samples (average: 4 cm^2).

3. Results and Discussions

3.1. Morphology, Structure, and Particle Size of GO and G-Sheets. The morphology, structure, and particle size analyses of GO and G-sheets by TEM, WAXD, and DLS analysis are presented in Figures 2(a)–2(d). The prolonged oxidation and exfoliation of GRT into GO sheets renders it with structural distortions with folding and wrinkling characteristics. The wrinkling and folding features of the nanostructured 2D graphene sheet assist in the attainment of thermodynamic stability [39, 43, 45]. Fortunately, these structural imperfections improve the mechanical properties of the elastomer-graphene composites because the distorted sheets confine, anchor, and restrict the mobility of the polymer chains [35, 43].

The wrinkled structure is restored upon reduction of GO by hydrazine into G-sheets (Figure 2(b)). Based on the TEM scale bar, G-sheets show an estimated thickness of ~0.5–5 nm. The particle size distribution of GO and G-sheets measured by the particle size analyzer (DLS) is presented in Figure 2(c). The hydrodynamic sizes (diameters) of the sheets dispersed in deionized water by a prolonged centrifuge are ~117 and ~114 nm for GO and G, respectively. Figure 2(d) shows the WAXD patterns of the fillers graphite (GRT), GO, and G, respectively. The GRT showed a very sharp diffraction peak observed at $2\theta = 26.5^\circ$ corresponding to an interlayer spacing of ~0.34 nm. This crystalline structure indicates closely packed layers of GRT sheets. The GO showed a peak at angle of $2\theta = 10.2^\circ$ (corresponding d-spacing of ~0.87 nm). Since d-spacing of GRT < GO, it implies there is an opening of the interlayer spacing of GO believed to be caused by the decoration of the galleries of GO sheets with water film and the oxygen moieties during the oxidation process [46–48]. A flat peak was observed for the case of G at $2\theta = 10.2^\circ$, instead a broader peak can be seen around $2\theta = 14 \sim 24^\circ$ and $2\theta = 15 \sim 23.4^\circ$, respectively, for G and GO sheets. These kinds of broad peaks suggest exfoliation of the sheets [35]. Further, a relatively sharper peak at the neck of the broader region of G-sheets which appeared around 21.5° (corresponding to d-spacing of 0.41 nm) is an indication of the presence of graphitic layers within the G-sheets. Therefore, it can be deduced that GRT cannot be converted into pure G-sheets via exfoliation and reduction of GO sheets. However, the resulting derivatives GO and G-sheets have proven to be effective nanostructured fillers for reinforcing rubber matrices to achieve the desired physico-mechanical properties [35].

3.2. Chemical Analysis of Nanoparticles and Rubber Compounds by FTIR. The FTIR spectra of the fillers (GO and G) and the vulcanizates of N, E, and N-E reinforced with the G and GO fillers are presented in Figures 3(a)–3(d) Also, the wavenumbers (cm^{-1}) and corresponding mode of vibration of the fillers and the various compounds are summarized in Table 2 with their remarks. A reduction of GO into G which leads to the disappearance and/or reduction of the peak intensities of the various oxygenated groups (C-OH, O-C=O, OH, and C-O-C) was observed as shown in Figure 3(a). Although, this observation confirms the reduction of GO into G sheets [35, 43], it must be emphasized that GO was not completely converted into pristine G-sheets due to structural defects and thermodynamic instabilities during the oxidation process and results in residual moieties of oxygen. The oxygen functionalities are relevant for forming composites with the elastomeric matrices [35, 43]. Figure 3(b) is the FTIR for the unfilled single matrix (N and E) and blends (N/E). The prominent absorbance with the vibrations in polypropylene (~722-751 cm^{-1}), ENB (~811-876 cm^{-1}) of E, and nitrile groups (~2235-2241 cm^{-1}) of N for both the single and blends are clearly represented and summarized in Table 2. It is interesting to observe that the peak for the alkyl group (C≡N) in N was absent for E which is normal. However, this peak was present in N and the blends (N/E). The peak intensities are in the order of N > B > C >A. Again, this peak was present for the filled blends in Figures 3(c)–3(d) but was absent for E-GO and E-G composites as shown in Figure 3(d). This confirms that the C≡N was not used up when the two (N/E) matrices reacted, a clear indication of immiscibility of N in E and vice versa as earlier reported [49–52]. Another significant observation can be seen in the samples with G and GO reinforcements which showed increased peak intensities at the vibrations of ~2357 cm^{-1} for the composites (Figures 3(c)–3(d). This could mean that GO and G may have taken part in the vulcanization process [35, 43, 53], and therefore, the differential scanning calorimetry (DSC) analyses further explains the miscibility of the blends in the next section.

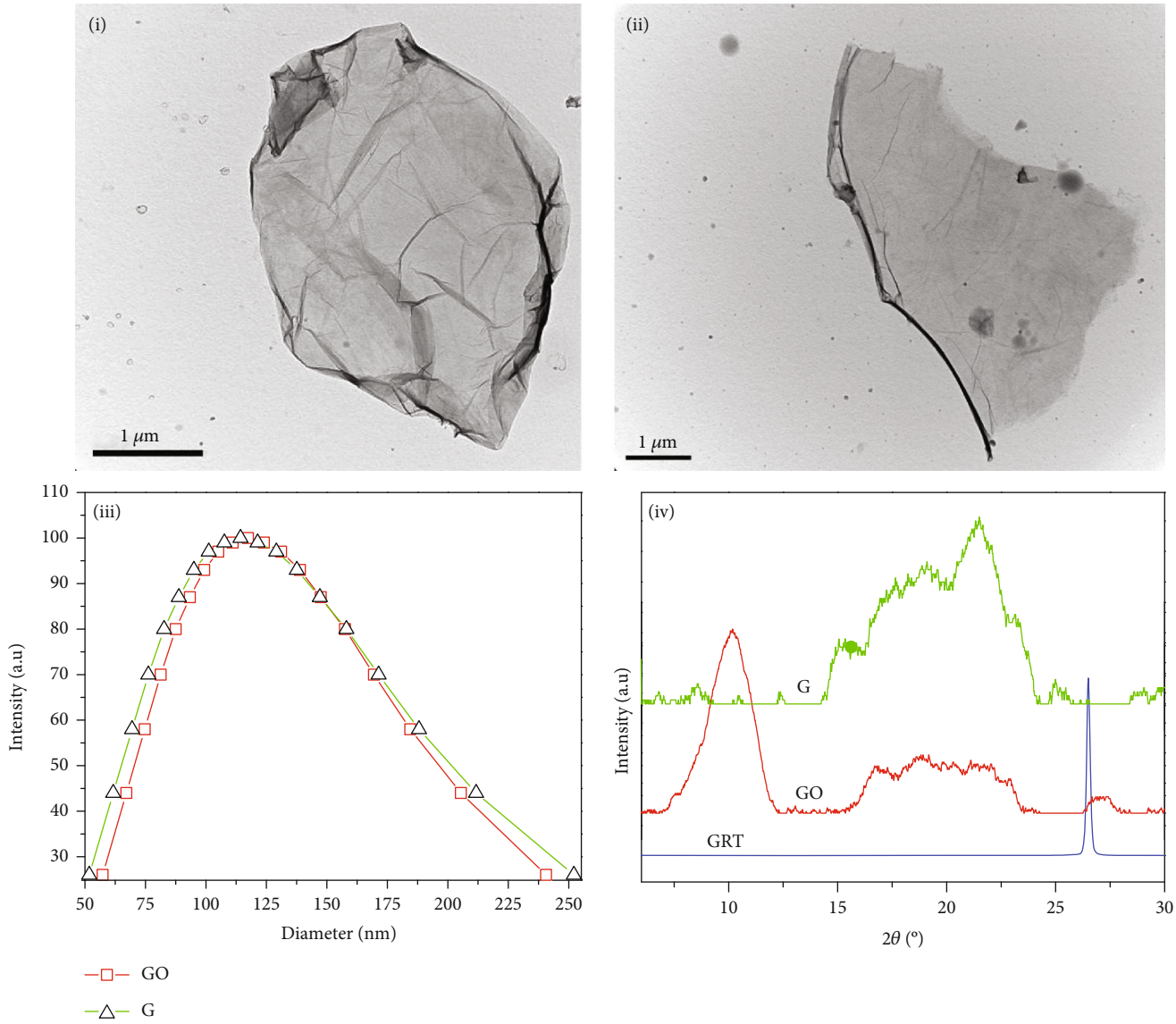

Figure 2: Characteristics of GO and GO sheets; (i) TEM image of GO-sheets, (ii) TEM image of G-sheets, (iii) dynamic light scattering (DLS) of GO and G-sheets, and (iv) wide angle X-ray diffraction analyses of GO, G, and GRT.

3.3. DSC Analysis. Figure 4(a) presents the glass transition temperatures (T_g) of only the pure matrix A (N/E) whilst Figure 4(b) represents the pure individual matrices (N and E), blends (A, B, and C), and their composites with GO and G, obtained from the DSC analyses. The individual pure matrices of N and E showed single T_g values at 40 and 45°C, respectively, which is within the T_g ranges (≤-40°C) for such elastomers [55]. The synergy effect of the individual matrices containing GO or G-sheets showed two distinct T_g values (T_{g1} and T_{g2}). In general, the first T_{g1} values are observed at high negative temperatures whilst the second T_{g2} values are seen at low negative temperature values. The T_{g1} results from the primary networks of N (N—S—S_x—N) and from the saturated E phase, which generally has a poor cross-linking reaction with sulfur, with the except of its ENB group (ENB—S—S_x—ENB) [17, 51, 55]. The higher T_{g2} values may be coming from the tighter structures of N chains with GO (N—S_x—GO—S_x—N) or with G (N—S_x—G—S_x—N) as well as the polar-polar interactions (—C≡$N^{\delta+}$———$O^{\delta-}$—H—GO) between acrylonitrile functions (—C≡N) of N and O-H of GO or G [43]. Zhao et al. [21] prepared a blend of (NR/N) (70/30) and observed two T_g; one round -64.5°C for NR and the -16.7°C for N, respectively, indicating that N has rigid structures compared to NR. Thus, by comparing the differences in the T_g of the elastomers, it clearly shows that the (N/E) blend in this current work was relatively immiscible, although the effect seemed to be lessened by the incorporation of the G and GO.

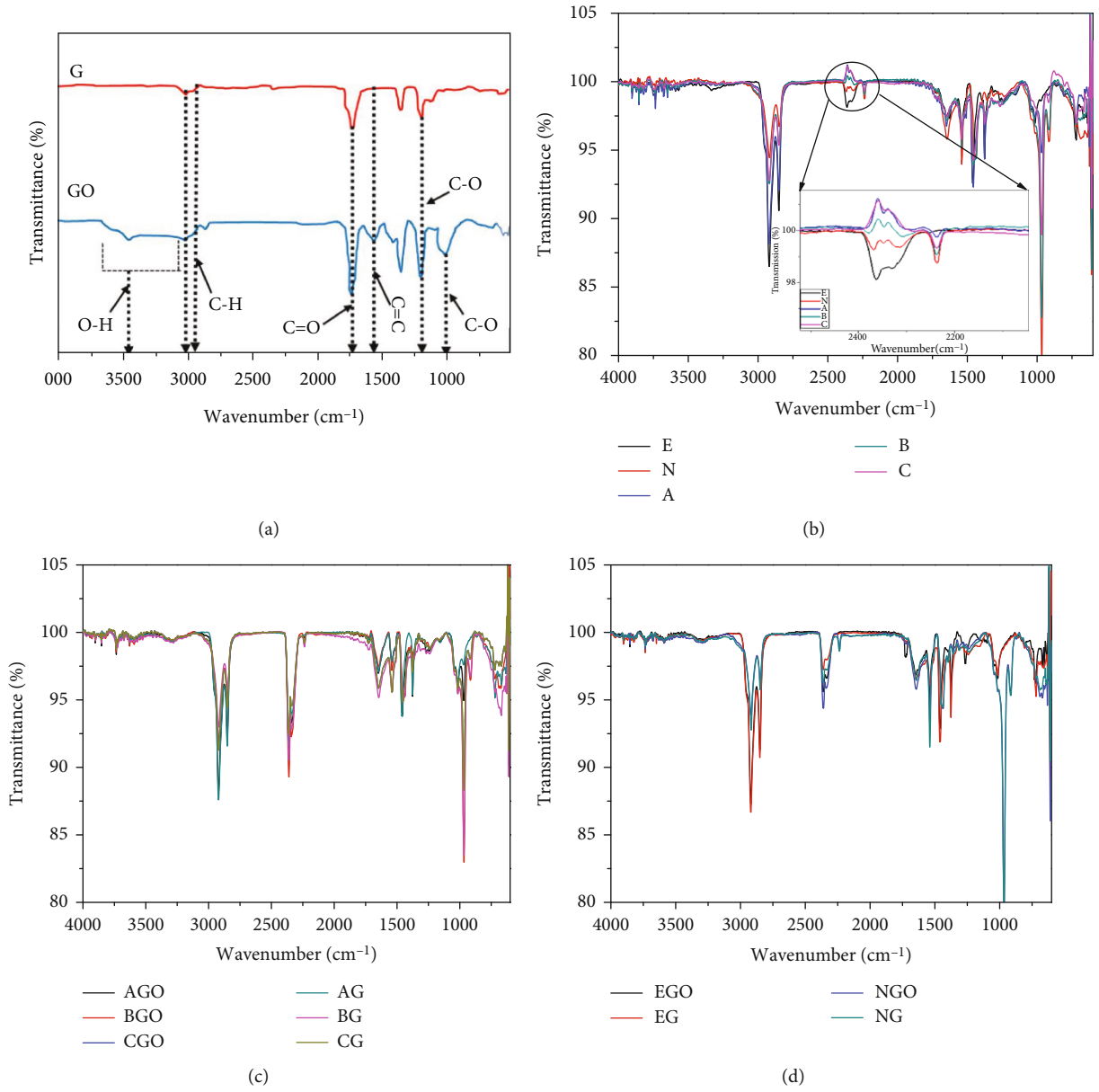

Figure 3: FTIR spectra of rubber compounds (a) GO and G, (b) unfilled-single and double matrices, (c) filled double matrices, and (d) filled single matrices.

3.4. Vulcanization Properties

3.4.1. Curing Time and Cure Rates. The vulcanization properties, onset of curing (t_{s2}), the optimum curing times (t_{90}), and the cure rate index (CRI) of N, E, the blends of (N/E), and their composites with GO and G are compared in Figures 5(a)–5(c)), respectively. In Figure 5(a), the unfilled and the nanocomposites rich in E generally lengthens the t_{s2}. Such delays in t_{s2} may be attributed to increase in viscosity which delays melting of the curatives to initiate crosslinking reaction as observed by Wu et al. [56] for NR-graphene composites. However, delays in t_{s2} is desired for the safety curing of the final product and its physico-mechanical properties [44, 55, 56]. Furthermore, the t_{90} shot up for compounds which contained higher content of E The slow sulfur curing behavior of the E-rich systems is due to the overall saturated nature of E, and therefore, E elastomers are cured using peroxide curatives [35, 51, 55]. However, the unsaturated portion of the diene of E makes sulfur curing possible [18, 19]. Therefore, an effective crosslinking of E system by sulfur crosslinker may depend on the content of ENB in the E structure.

In comparison, the GO-based systems delayed the curing times of the N, E, and (N/E) matrices relative to their counterparts reinforced with G. The GO is reported to act as scavenger of the cure accelerators during crosslinking reaction [53]. Apart from the primary crosslinking reactions such as ENB—S—S_x—ENB and N—S—S_x—N by the sulfurating species, the numerous oxygen species (C-OH, O-C=O, OH, and C-O-C) activate on the GO and G sheets to engage

Table 2: FTIR spectra of fillers, pure matrices, the blends, and their composites with the fillers.

Wavenumber (cm^{-1})	Possible vibration bands/remarks
Fillers	
3000~3700	O–H stretching vibration, showing the hydrophilic nature of GO [48]
1742	The C=O stretching vibration of COOH groups at the edges of GO [43, 48]
1219	Attributed to stretching vibration peaks of R–O (epoxy) [35, 48]
1039	Attributed to stretching vibration peaks of R–O (alkoxy) [48]
1576	Attributed to the skeletal vibration of the G sheets [35, 48]
Unfilled and filled compounds	
751 and 722	Wagging vibration of $-(CH_2)_n-$ groups in the PP, where $n \geq 5$ [52, 54]
811-876	Vibration of the unsaturated C=C groups in ENB structure [52, 54]
963	The C–H wagging motion vibrations of butadiene [52, 54]
1376	Symmetric bending vibration of $-CH_3$ group in PP unit [52, 54]
1459	Rocking vibration of $-CH_2$ group in PP unit [49–52]
2235-2241	Stretching vibrations of alkyl group (C≡N) in NBR [54]
2849	Symmetric C–H stretching vibrations (aliphatic CH_2 group) [52, 54]
2918	Asymmetric C–H stretching vibration (aliphatic group) [52, 54]

in a secondary crosslinking reactions with the ENB part of the E and the unsaturated part of N as depicted in Figure 6 (i). Furthermore, co-crosslinking reaction between the ENB part of E and N (ENB—S—S_x—N) is also possible as depicted in Figure 6 (ii). Thus, the delays in the overall crosslinking reaction of the compositions were expected [53, 55].

Another fascinating observation that is worth stressing is that the N-GO compounds recorded faster crosslinking reaction in terms of t_{s2}, t_{90}, and CRI when compared with N-G, E-G, and E-GO as well as the respective unfilled and filled blends. This observation suggests that the polar moieties on GO graphene sheets essentially act more as cure accelerators in a polar environment than as retarders when in nonpolar rich phase. The curing property (CRI) obtained in the current results outperformed those recently reported by Tawfic and Hussein [17], Mayasari et al. [18], and Paran et al. [19] who adopted open two-roll mixing in processing elastomers. Therefore, the solution mixing method has proven to be an effective method for processing elastomeric blends consisting of different polarities, even in the absence of compatibilizer.

3.4.2. Torque Properties. The minimum torque or viscosity index (M_L), maximum torque (M_H), and the strength index ($\Delta M = M_H - M_L$) of unfilled and blends are presented in Figures 7(a)–7(b). Generally, the compounds rich in E show higher values of M_L, M_H, and ΔM than those with lowly filled with E content. This includes the N and E matrices reinforced with G and GO sheets. It can again be observed that the nanocomposites showed higher torque properties than the pristine elastomers. Such increments are due to restrictions in mobility of the E chains and the tight networked structures introduced by the GO/G during the crosslinking reaction [55, 57]. The enhanced torque values generally result in higher mechanical properties of the corresponding rubber compounds [16, 44, 58, 59]. However, they are dependent on the processing parameters, filler-filler, polymer-filler networks, and primary chain-chain interactions [60, 61].

3.5. Tensile Properties. The tensile properties (ultimate tensile strength UTS (MPa) and elongation at break, E_{br} (%)) deduced from stress-strain analyses for the various compounds are compared in Figure 8(a)). It can be seen in Figure 8(a) that the 20 phr N-80 phr E was very crucial for the blend formation as it yielded the highest UTS value compared with the unfilled N and E, the N-E, as well as their composites with GO and G. For instance, the blend A attained UTS value of about ~10 and ~127% greater than N and E, respectively, whilst leading B and C by ~22 and ~14%, respectively. For the composites, N-GO exhibited the highest UTS properties than the rest of the compositions, as N-GO attained about ~5, ~123, and ~23% rise in UTS than N, E-GO, and N-GO, respectively. On comparing the UTS; N-based compounds outperformed that of the E systems for both the filled and unfilled compositions. This can be attributed to the primary sulphur networks (N—S—S_x—N) (ENB—S—S_x—N) and the additional networked structures created by the graphenes (N—S—GO—S_x—N) and (—C≡$N^{\delta+}$———$O^{\delta-}$—H—GO) within the N-rich compounds as observed in our earlier work [53]. The E_{br} (%) of the single, double filled and unfilled compositions are shown in Figures 8(c) and 8(d). Although no clear trend can be seen, yet it was obvious that unfilled and filled blend N generally showed desired E_{br} (%) values compared to the rest of the samples, for example, N-GO was 32% higher than N and ~147%, ~153%, and~150% higher than E, E-GO, and E-G composites, respectively. Also, N-GO got an increment of ~17%, ~216%, and ~44% than N, N-GO, and N-G, respectively. Thus, whether filled or unfilled, it appeared formation of blend between E and N required smaller amount of N forming a dispersed phase within a continuous phase of E as it was clear that higher content of N did not benefit the blend formation. Again, the compounds filled with GO obtained improved tensile properties than those of G, especially when the blends were considered. This was due to additional network density created by the oxygen moieties of GO (C-OH, O-C=O, O-H, and C-O-C) and the matrix [62, 63]. The current tensile property results obtained for the N/E blends prepared via solution mixing approach were comparable and mostly better than the results obtained for N/E blend prepared by melt mixing technique reported in recently by Paran and Mayasari et al. [18, 19]. Further,

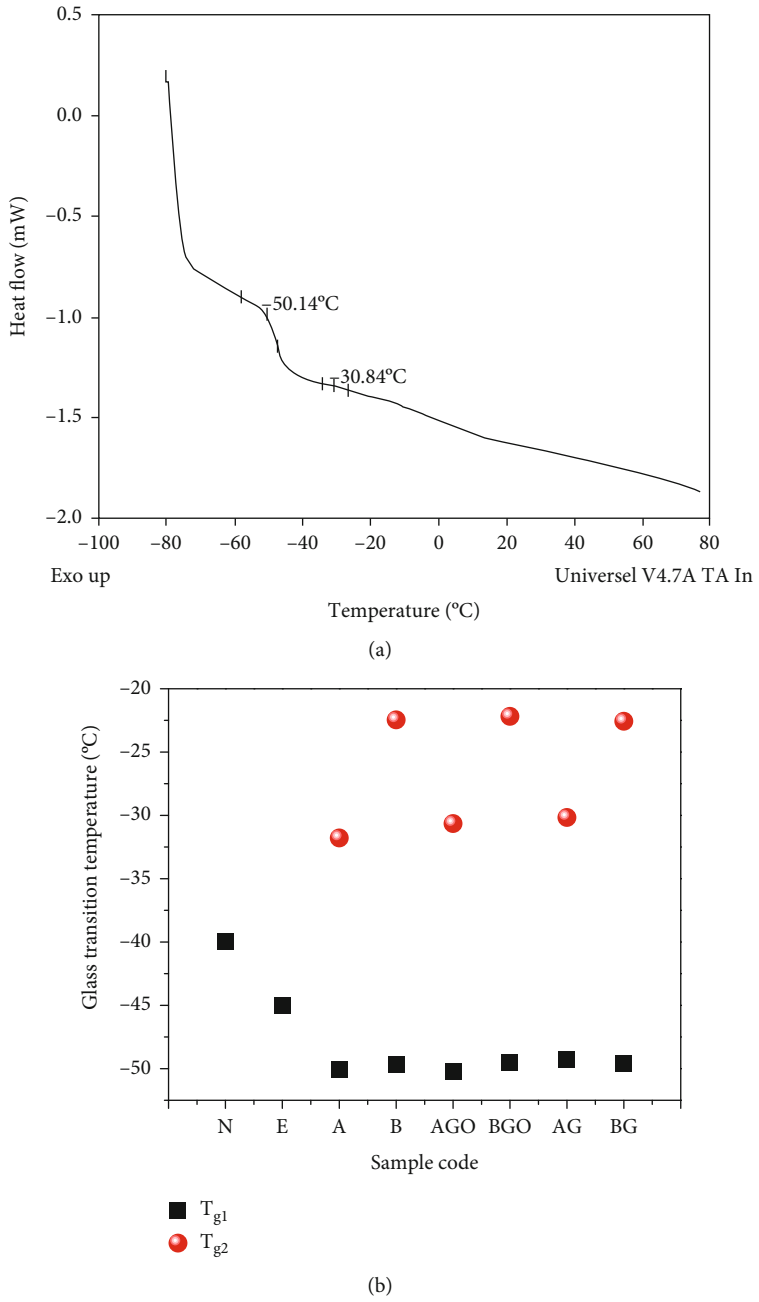

Figure 4: Glass transition temperatures (T_g); (a) the T_g for representative samples (a) and (b) comparing the T_g results for representative samples of unfilled and filled compounds.

Tawfic and Hussein [17] earlier succeeded in enhancing the immiscibility nature of N/E blends by incorporation of variable amount of Am-Ep compatibilizer (0-10 phr) into the blend comprising 50/50 by using melt mixing method. Interestingly, the unfilled blends of the current work (A, B, and C) showed better tensile strength compared to those filled with the Am-Ep compatibilizer by Tawfic and Hussein [17]. In particular, the unfilled blend C (50/50) of this present work obtained about 111 and 48% compared with the unfilled 50/50 and 50/50 filled with optimized amount of 7.5 phr Am-Ep compatibilizer. It must be stated/established here that many factors might have contributed to this improvement; however, the solution technique employed was suspected to have yielded effective mixing level leading to desired cocuring and physical chain entanglements between the polar and nonpolar phase with or without the presence of the graphene sheets (GO and G).

3.6. Dielectric Properties

3.6.1. Dielectric Constant. The dielectric property of a material is defined such that, when an external electric field say E_x is applied to a dielectric-to-be material, the disoriented dipoles molecules within the materials align themselves

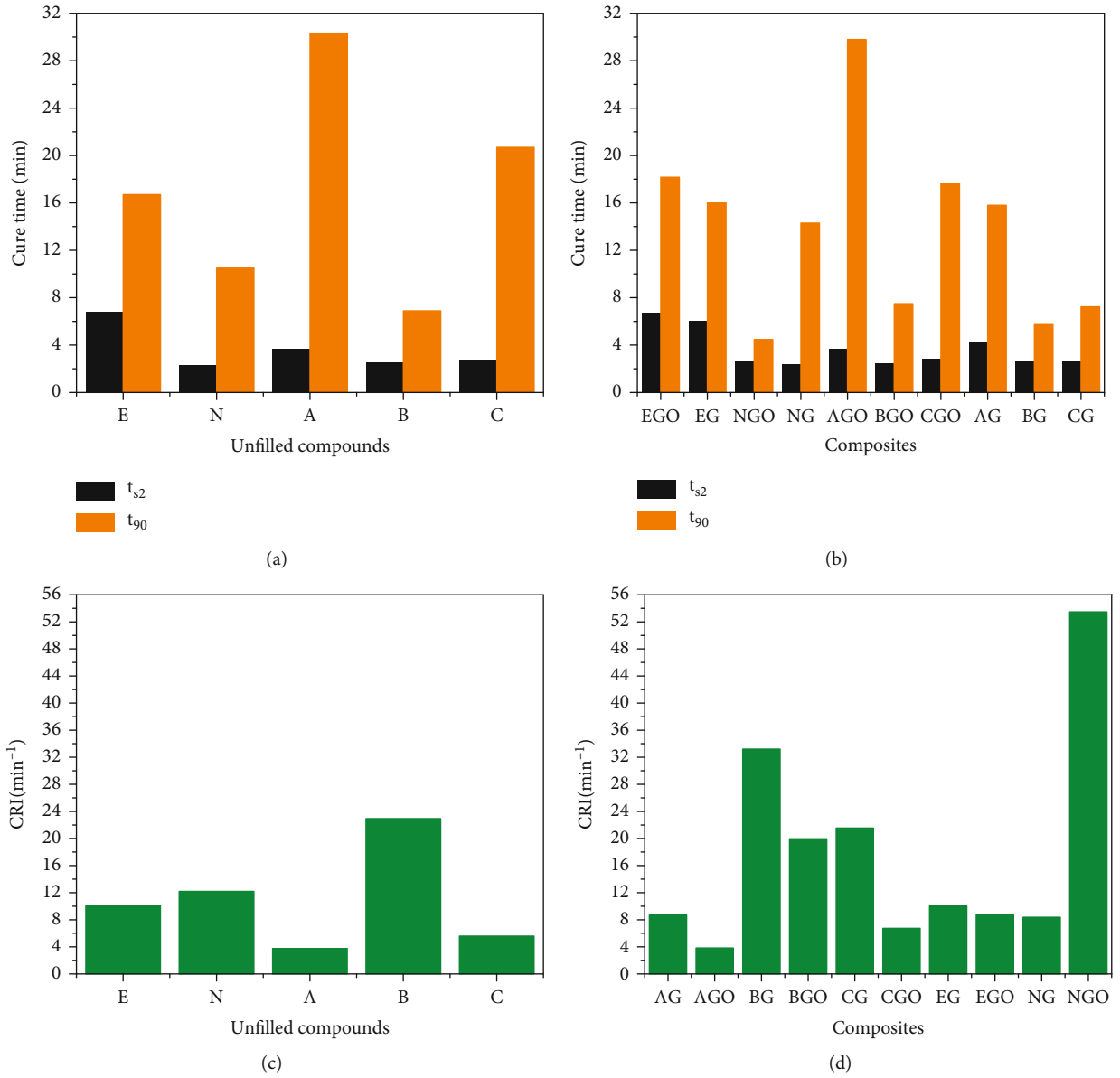

Figure 5: Cure properties of N- and E-based compounds. (a) Cure time for unfilled single and double matrix, (b) cure time for filled single and double matrix, (c) cure rate index for unfilled single and double matrix, and (d) cure rate index for filled-single and double matrix.

towards the E_x. In this way, the internal field induced by the dipole molecules in the material opposes the E_x thereby reducing the net electric field and the material thus becomes dielectric [64, 65]. The influence of frequency and filler on the dielectric constant (ε') of the single matrices (E and N), the unfilled blend (A, B, and C), and the filled blend (N-GO, N-G and E-GO, and E-G) have been presented in Figures 9(a)–9(c). Clearly from Figure 9(a), the matrix rich in N (polar matrix phase) recorded higher values of ε' as compared to those loaded with smaller amount of N (non-polar matrix phase). Thus, the single matrix (N) gained the highest ε' than its counterpart E and E-rich blends. For example, at zero frequency, N attained over 283, 283, 46%, and 156% in ε' than E, A, B, and C, respectively. The inclusion of GO and G into matrices further raised the ε' value for the N-rich compositions for the single and the double matrix. In comparison, N-G and N-GO obtained 317 and 283% increment in ε' than E-G and E-GO, respectively, as shown in Figure 9(b). Similarly, for the double matrix composites, the ε' of the N-rich compositions (BGO and BGE) still dominated other samples as seen in Figure 9(c). A number of factors including ionic nature and the radicals from the compounding components of vulcanized rubber improved electrode polarization which is a surface effect [66] and/or Maxwell-Wagner-Sillars interfacial polarization may influence the ε' of the bulk material [64, 65, 67]. It appears the presence of the polar moieties (—C≡N) in N contributed hugely to the increase in ε', especially for the N-rich compounds. Thus, a reduction in polarity of the compositions due to reduction in the concentration of the

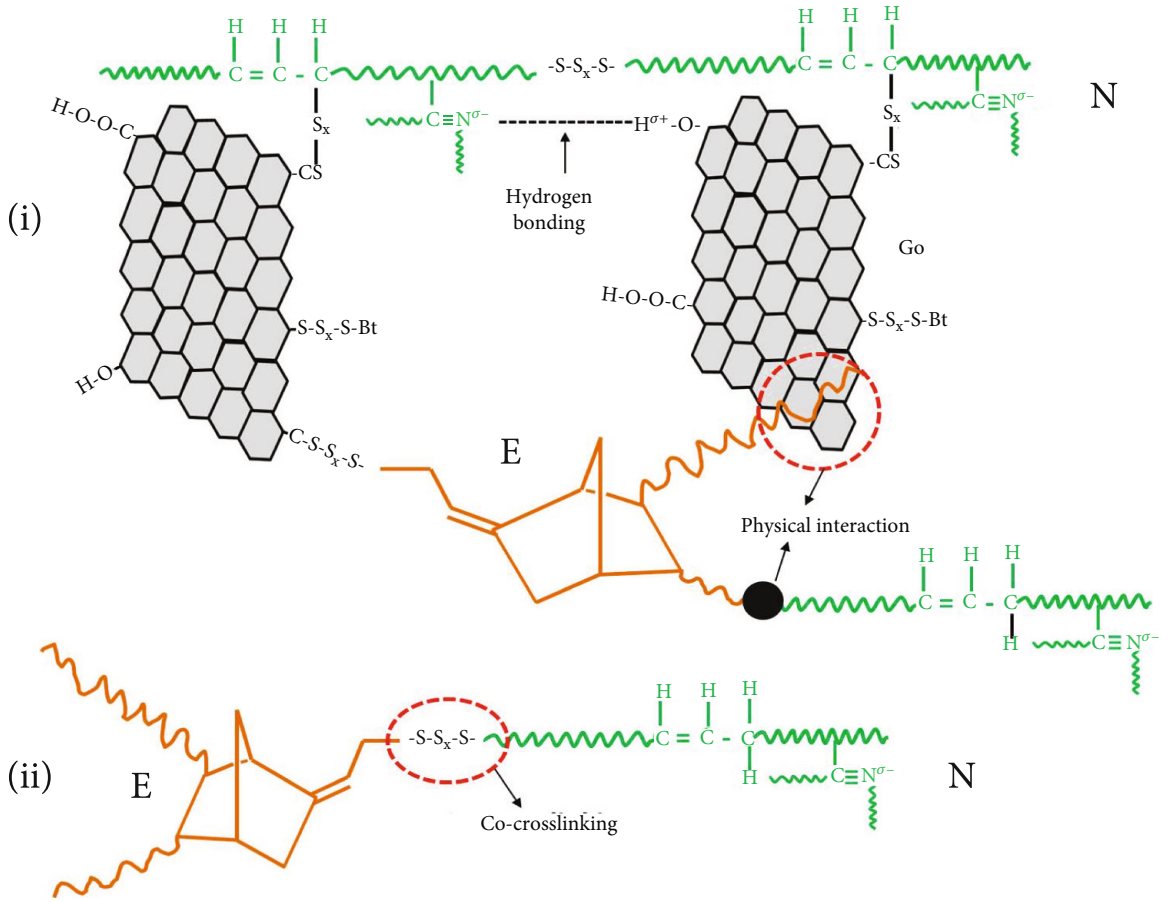

Figure 6: Interactions of GO and G sheets with N and E matrices during vulcanization; (i) reaction of GO/G fillers, N, and E matrices and (ii) cocrosslinking between N and E.

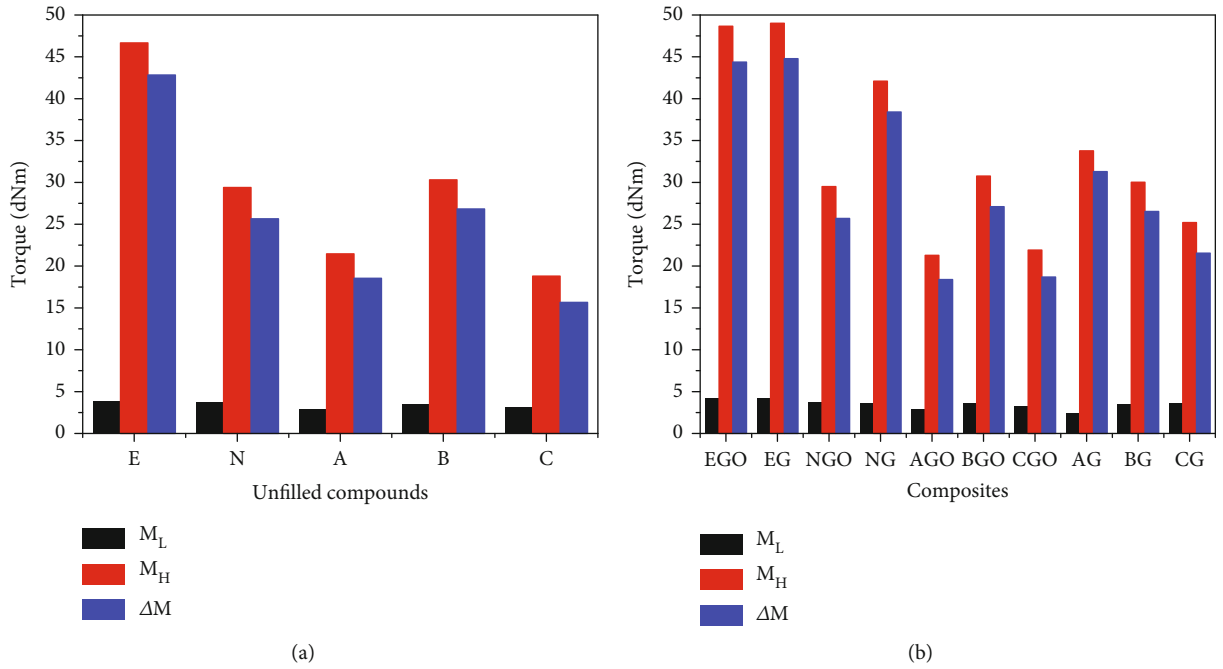

Figure 7: Torque properties of the single, blends, and their composites with GO and G. (a) The unfilled matrices of the single and blend; (b) filled matrices of the single and blend.

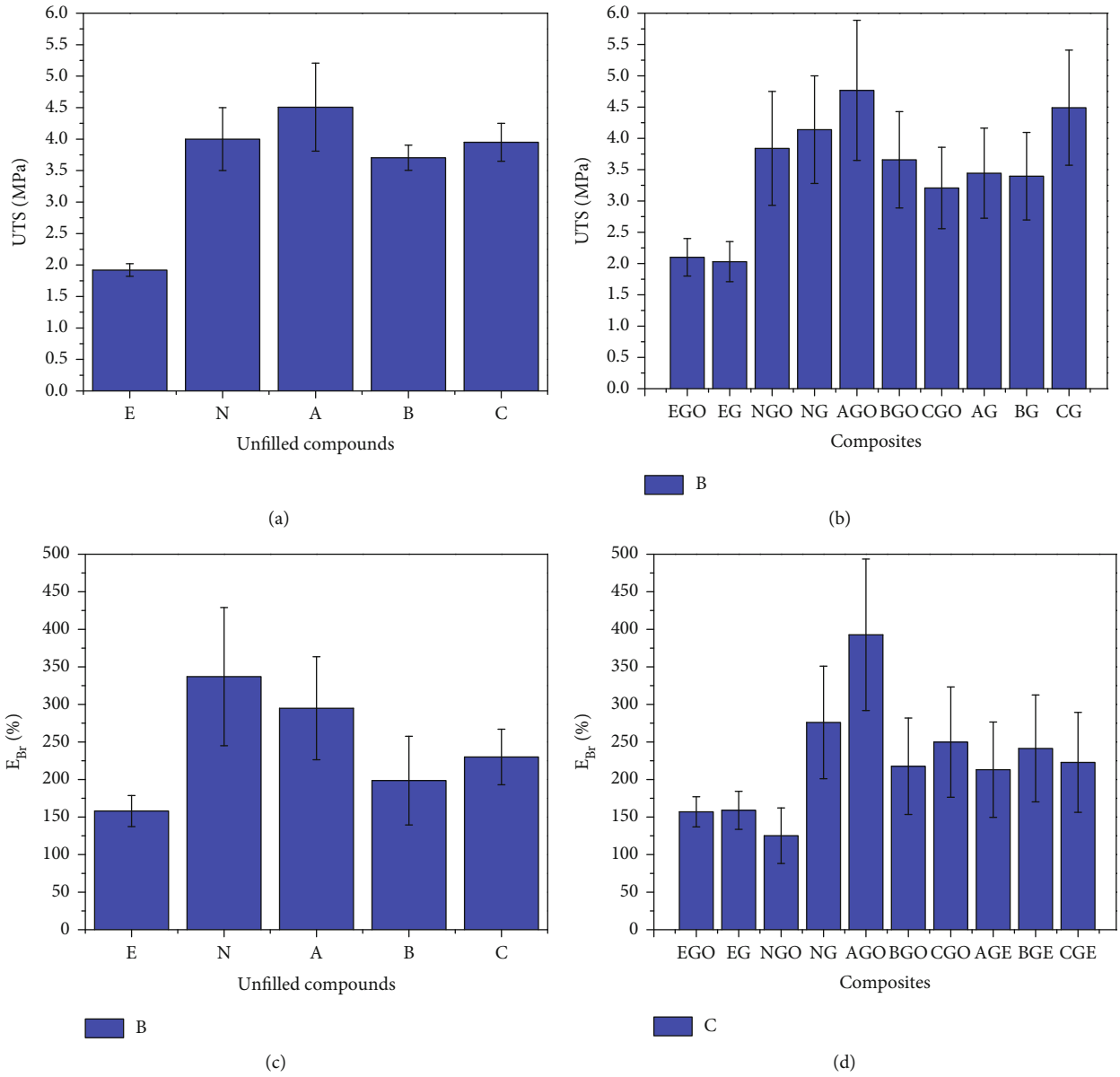

Figure 8: Tensile properties of unfilled and filled compounds/blends. (a) Tensile strength of unfilled-single and double matrix; (b) tensile strength of single and double matrix-filled GO and G; (c) elongation at break of single and double matrix-filled GO and G; (d) elongation at break of single and double matrix-filled GO and G.

polar phase accounted for the inferior ε' for the blends. Hence, the order of decreasing strength of the ε' is 100-(N) > 80-N-20-E (B) > 50-N-50-E (C) > (20-N-80-E (A) > 100-E (E). In addition, the internal electric field generated by the inclusion of GO and G further increased the net polarization of the compositions as was reported for electrical conductive particles like nanotubes (CNTs) by Das-Gupta and Scarpa [22], carbon blacks (CB) Barber et al. [66], and metallic particles, Wang et al. [68]. The G-sheets are closely related to the pristine graphene sheets which are rich in delocalized electrons in the $\pi - \pi$ structures, well known for high electrical conductivity [29–31]. In contrast, the results for the current study exhibited enhanced ε' behavior than N-GO and N-GOAu earlier reported [34, 44]. Even at lower concentrations of GO and G (0.1 phr), an appreciable ε' was obtained for the N-rich compounds than that of polydimethylsiloxane (PDMS) filled with 1~5 phr GO by Wang et al. [68], butyl rubber-carbon nanotube (2~6 phr) composites by Dang et al. [69] and NR-CB (50 phr) with variable amount (1~5 phr) of graphene nanoparticles by Al-Hartomy et al. [27]. Furthermore, the ε' properties for the current compositions have significantly improved compared with prior reports by Paran et al. [19] whose compositions recorded ~2.36 and ~2.52 values ε', respectively. With the effect of frequency, a high value of ε' is observed at low frequency region whilst relatively low ε' is seen at higher frequency region. The alternation of the field is slow in the low frequency region, and this provides sufficient time to

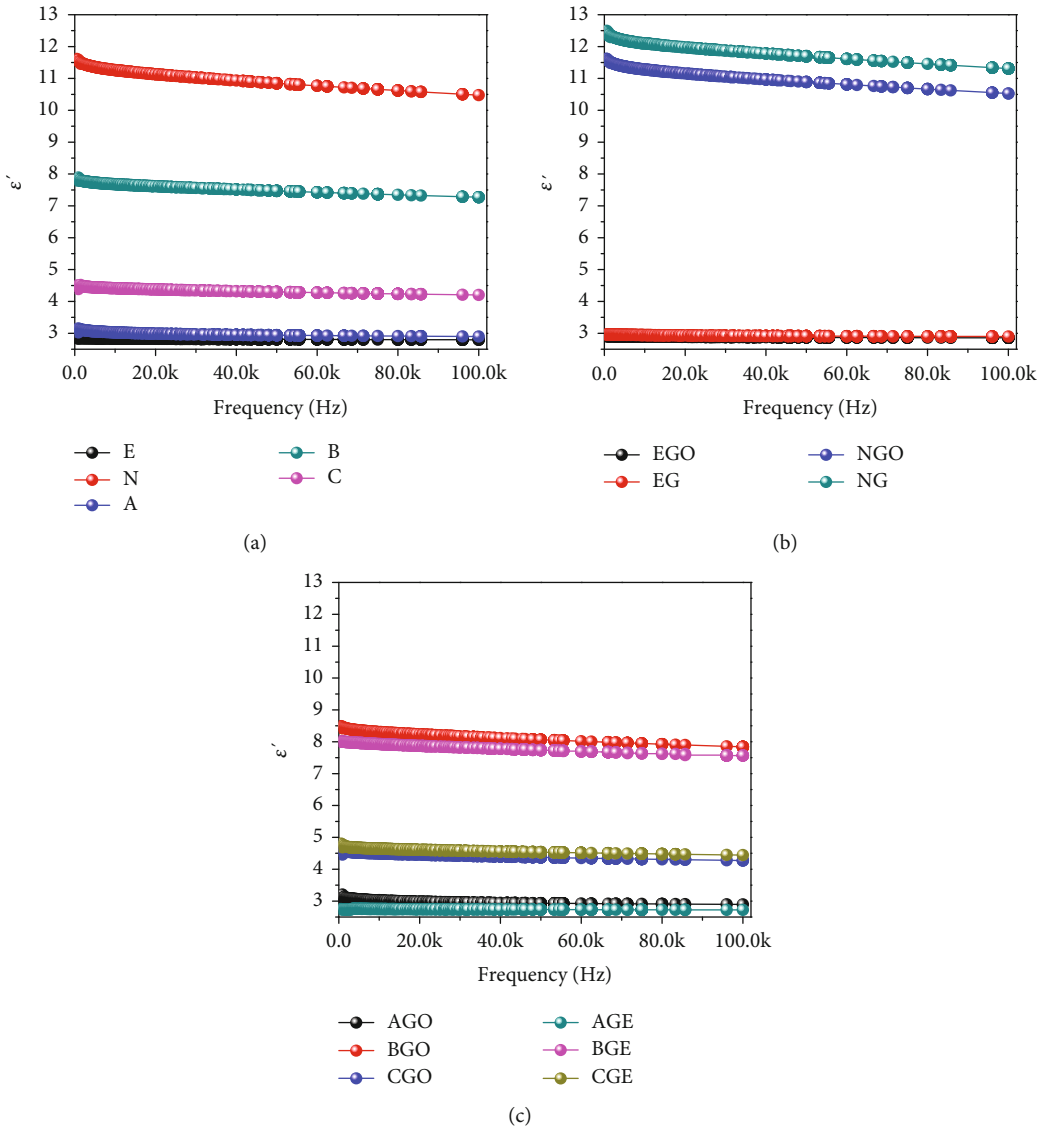

Figure 9: The effect of frequency and filler on the dielectric constant of (a) unfilled single and double matrix, (b) single matrix-filled GO and G, and (c) double matrix-filled GO and G.

permanent and induced dipoles to align themselves according to the applied field, which leads to boosted polarization [70]. Nevertheless, the low ε' at higher frequency region is a common and expected behavior in most dielectric materials and has been linked to dielectric relaxation which is suggested to be the cause of anomalous dispersion [33, 34, 70]. The dielectric relaxation involves the orientation polarization which in turn depends upon the molecular arrangement of material under study for dielectric material [71, 72]. Earlier, Dang et al. [73] established that at high frequency region, there is a competition of higher electrical field and increased frequency which results in low ε'. This observation was recently reported in poly(vinyl alcohol) reinforced with graphite and GO recently [70] and poly(vinylidene fluoride)/exfoliated graphite nanoparticle composites [74].

3.6.2. Loss Factor. One of the important factors to consider in developing dielectric materials for energy storage and electric field grading is the loss factor or loss tangent (tan δ) [75, 76]. For this reason, the tan δ of the dielectric-to-be-materials has been compared in Figures 10(a)–10(c) as a function of frequency. In Figure 10, the tan δ generally increases as the frequency increases. As can be seen, the E-rich compounds show lower tan δ with lesser energy dissipations. The neat E compound shows about 1560% improvement than the neat N at high frequency of about 100 KHz. The order of decreasing of energy dissipation for the unfilled compounds is given by N (100 phr of N) < B (80 phr N and 20 phr of E) < C (500 phr N and 50 phr of E) < A (20 phr N and 80 phr of E) < E (100 phr of E). One remarkable observation is that when G-sheets were incorporated into N matrix, the tan δ dropped significantly to ~84% for NG as seen in Figure 10(b). However, this observation was missing for the GO-filled compounds.

In Figure 10(c), some scattering can be seen for the composite blends, but the overall trend is that the G-sheet-filled

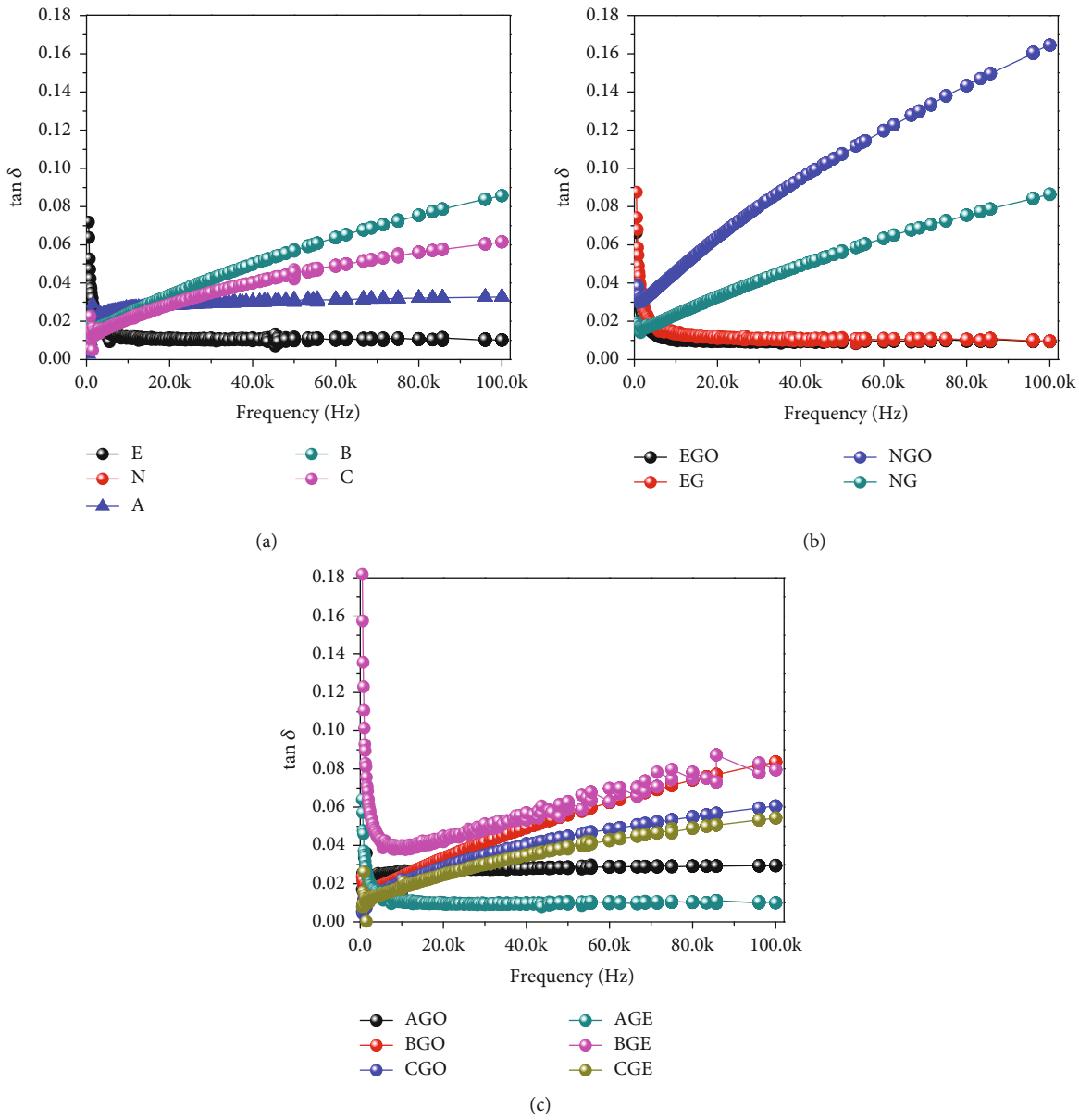

Figure 10: Loss factor of (a) unfilled single and double matrix, (b) single matrix-filled GO and G, and (c) double matrix-filled GO and G.

compounds lower energy dissipation than the GO-based compounds. Again, the E-rich compound filled with G-sheets (AG > BG > CG) showed relatively lower tan δ than the unfilled blends (A > B > C). Interestingly, comparable results of the tan δ between the unfilled and the GO-filled compounds can be seen. The high conductivity of the G-sheets than GO sheets [35, 55] may be responsible for this and therefore can be concluded that the E-rich compounds offer better advantage in lowering losses in energy storage applications with minimal losses than the N-rich counterparts.

3.6.3. Dielectric Modulus. Earlier, the dielectric modulus ($M^* = 1/\varepsilon'$) was adopted to study the charge relaxation phenomena [77, 78], and since then, many theories have been proposed in explaining the quantity M^* of different materials [79, 80]. As an effective tool, the value of M^* has been used to study the relaxation behavior of dielectric-to-be materials. In practice, M^* corresponds to the relaxation of the electric field in the material at a constant electric displacement; hence, the electric modulus characterizes the real dielectric relaxation process which can be expressed in

$$M*(\omega) = \frac{1}{\varepsilon'(\omega)} = M' + iM'' = M\infty\left[1 - \int_0^\infty \left(-\frac{d\varphi(t)}{dt}\right)\exp(-i\omega t)dt\right], \quad (4)$$

where M_∞ is the asymptotic value of $M'(\omega)$ and $\phi(t)$ is the time evolution of the electric field within the material. In this present work, $M*$ was directly computed by taking the inverse of the ε' obtained from the experiment for the

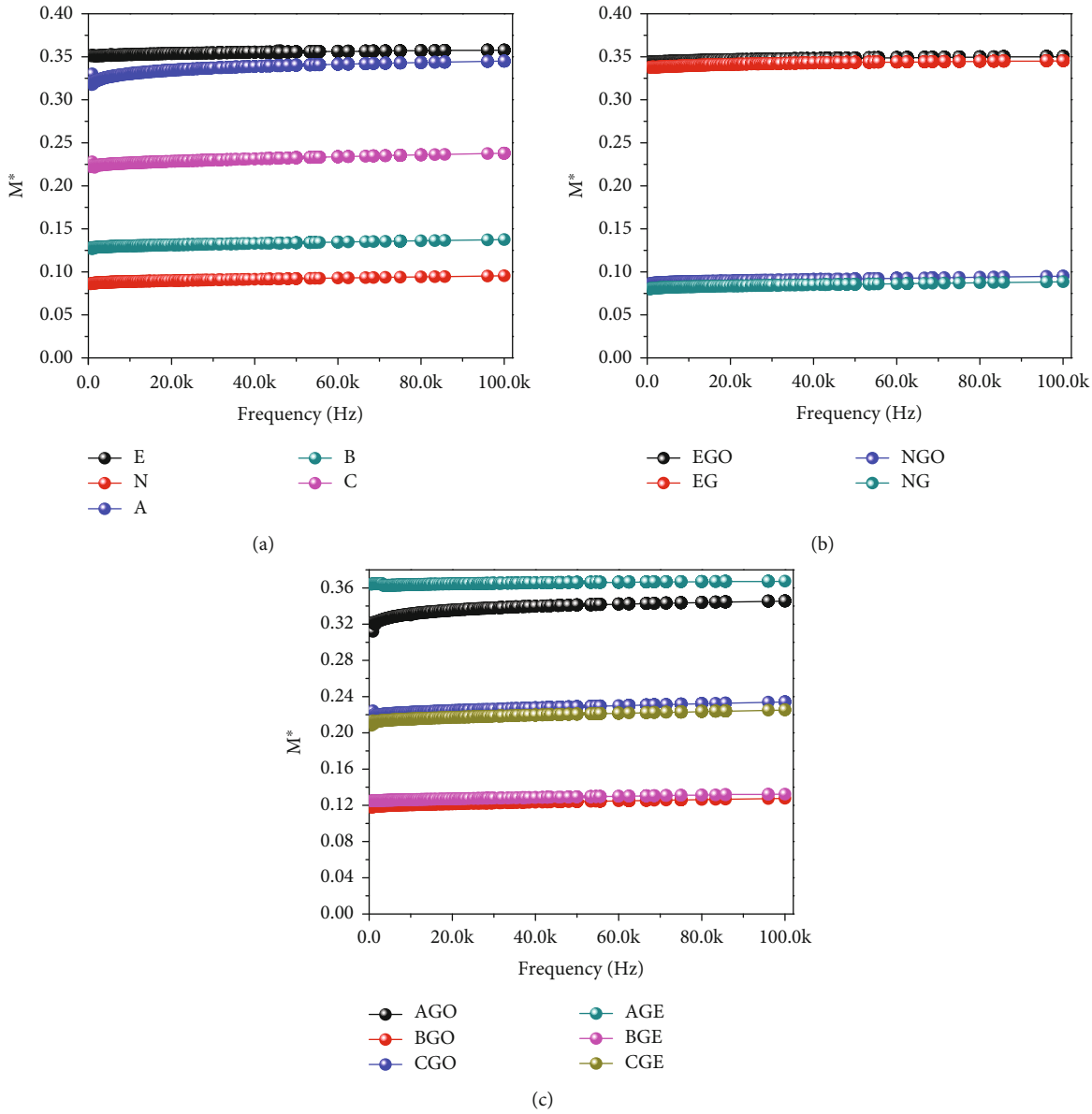

Figure 11: Dielectric modulus of (a) unfilled single and double matrix, (b) single matrix-filled GO and G, and (c) double matrix-filled GO and G.

various compositions. Figures 11(a)–11(c) compares the plot of $M*$ as a function of frequency for the various compositions. At room temperature, higher than the T_g of the various compounds, the N-rich compositions showed lower M^* values compared to the E-rich compositions, for the unfilled single and double matrices (Figure 11(a)). Also, for the GO/G-filled compounds, it was seen that G-sheet-based composite show lower M^* than GO-based systems as frequency increases. The decrease in M is associated with the decay of the electric field caused by strong polarity of the matrix and the additional carrier charge mobility of incorporated conductive fillers [23]. Meanwhile, the high polar groups relaxing at the vicinity of the GO/G-sheets also contributed to lower M^*. The relaxation behavior of epoxy observed above T_g was linked to the hopping of ions in the matrix according to Tian and Ohki [78]. In this work, at the same filler loading of 0.1 phr, the tighter structures (N-rich matrix or the N-rich in the cocrosslinked phases of the blend) associated with restricted chain mobility and T_g might show a broad relaxation mode rather than Debye mode well noted for liquids [24]. Similarly, a stronger linear correlation between CB loading in E matrix and the M^* was established, and it revealed a non-Debye type of relaxation (broad relaxation behavior) for E-CB composites [23].

4. Conclusions

The blend of ethylene-propylene-diene-monomer (EPDM) represented as E and acrylonitrile rubber (NBR) denoted as N was prepared by using a combination of solution and

open-roll mixing method for the first time. A composite of the single matrix and the blends with graphene oxide (GO) or reduced graphene oxide sheets (G) were separately formed. The E-rich compounds were found to delay crosslinking reactions, owing to their saturated nature. The N-rich compounds generally demonstrated improved tensile properties than the rest of the compositions. This was linked to numerous networked structures created in the presence of the graphene sheets (N—S—GO—S_x—N), (N—S—G—S_x—N), (—C≡$N^{\delta+}$———$O^{\delta-}$—H—GO), and (—C≡$N^{\delta+}$———$O^{\delta-}$—H—G) besides the primary networks (N—S—S_x—N) and cocrosslinking structures (ENB—S—S_x—N) between E and N. These structures restrict the mobility of the chains in the N-rich phases of the blends, thereby improving mechanical properties. However, composition AGO exhibited the highest strength and elongation at break properties (%), noted as the optimized composition in terms of tensile properties. The N-rich compounds also exhibited high dielectric constant due to the presence of the polar moieties (—C≡N) of N and that polar-polar interactions with the graphene (—C≡$N^{\delta+}$———$O^{\delta-}$—H—G) noted for high electrical conductivity. Contrary, the N-rich compounds showed relatively poor energy dissipation when compared with E-rich compounds. The solution mixing method was confirmed to be a very effective method for forming rubber blends involving polar and nonpolar matrices, even in the absence of compatibilizers. Finally, the results obtained provide insights on how tailored rubber blends reinforced with GO or G-sheets can be used to form composites which have high tendency to improve dielectric constants, mechanical properties, and for energy storage systems with minimal losses.

Data Availability

Data can be available on request from authors.

Conflicts of Interest

The authors declare no competing financial interest. The corresponding author have consent from all co-authors.

Acknowledgments

We thankfully acknowledge the support from Professor Changwoon Nah (Intelligent Polymer Nano-materials Lab) of Polymer Nano-science and Technology Department, Jeonbuk National University, for allowing us to use their facilities for our studies. We also acknowledge the Office of Research, Innovation and Development (ORID) of University of Ghana for making this study successful. This work is self-funded.

References

[1] A. Das, D.-Y. Wang, K. W. Stoeckelhuber et al., *Advanced Rubber Composites*, G. Heinrich, Ed., Springer-Verlag, Berlin Heidelberg, 2011.

[2] M.-J. Jiang, Z.-M. Dang, and H.-P. Xu, "Giant dielectric constant and resistance-pressure sensitivity in carbon nanotubes/rubber nanocomposites with low percolation threshold," *Applied Physics Letters*, vol. 90, no. 4, article 042914, 2007.

[3] H. K. Joseph, *Polymer Nanocomposites: Processing, Characterization, And Applications*, McGraw-Hill, USA, 2006.

[4] S. Anandhan and S. Bandyopadhyay, "Polymer nanocomposites: from synthesis to applications," *Nanocomposites And Polymers With Analytical Methods*, vol. 1, 2011.

[5] S. Kim, J. Oh, J. Lee, Y. Yoo, M. Bismark, and C. Nah, "Preparation and performance of bubble-type actuator for Braille display," *Advanced Materials Research*, vol. 875-877, pp. 1516–1519, 2014.

[6] B. Mensah, D. Kumar, G.-B. Lee, J. Won, K. Gupta, and C. Nah, "Gold functionalized-graphene oxide-reinforced acrylonitrile butadiene rubber nanocomposites for piezoresistive and piezoelectric applications," *Carbon Letters*, vol. 25, pp. 1–13, 2018.

[7] F. R. Al-solamy, A. A. Al-Ghamdi, and W. E. Mahmoud, "Piezoresistive behavior of graphite nanoplatelets based rubber nanocomposites," *Polymers for Advanced Technologies*, vol. 23, no. 3, pp. 478–482, 2012.

[8] P. D'Ambrosio, D. De Tommasi, D. Ferri, and G. Puglisi, "A phenomenological model for healing and hysteresis in rubber-like materials," *International Journal of Engineering Science*, vol. 46, no. 4, pp. 293–305, 2008.

[9] W. Luo, X. Hu, C. Wang, and Q. Li, "Frequency- and strain-amplitude-dependent dynamical mechanical properties and hysteresis loss of CB-filled vulcanized natural rubber," *International Journal of Mechanical Sciences*, vol. 52, no. 2, pp. 168–174, 2010.

[10] Z. F. Liu, S. Fang, F. A. Moura et al., "Hierarchically buckled sheath-core fibers for superelastic electronics, sensors, and muscles," *Science*, vol. 349, no. 6246, pp. 400–404, 2015.

[11] Y. Lin, K. Wu, Y. Liu, L. Wang, and M. Guo, "Dielectric spectroscopy of aluminium hydroxide particles filled silicone rubber and dielectric model analysis with modified numerical solutions," *Journal of Physics D: Applied Physics*, vol. 53, no. 27, article 275303, 2020.

[12] M. Maiti and A. K. Bhowmick, "Effect of polymer–clay interaction on solvent transport behavior of fluoroelastomer–clay nanocomposites and prediction of aspect ratio of nanoclay," *Journal of Applied Polymer Science*, vol. 105, no. 2, pp. 435–445, 2007.

[13] A. Boonmahitthisud and S. Chuayjuljit, "NR/XSBR nanocomposites with carbon black and carbon nanotube prepared by latex compounding," *Journal of Metals, Materials and Minerals*, vol. 22, no. 1, 2012.

[14] B. Mensah, H. G. Kim, J.-H. Lee, S. Arepalli, and C. Nah, "Carbon nanotube-reinforced elastomeric nanocomposites: a review," *International Journal of Smart and Nano Materials*, vol. 6, no. 4, pp. 211–238, 2015.

[15] B. Mensah, S. Kim, D. H. Lee, H. G. Kim, J. G. Oh, and C. Nah, "Autohesion behavior of brominated-isobutylene-isoprene gum nanocomposites with layered clay," *Elastomers and Composites*, vol. 49, no. 1, pp. 43–52, 2014.

[16] C. Nah, S. G. Kim, G. S. Shibulal et al., "Effects of curing systems on the mechanical and chemical ageing resistance properties of gasket compounds based on ethylene-propylene-diene-termonomer rubber in a simulated fuel cell environment," *International Journal of Hydrogen Energy*, vol. 40, no. 33, pp. 10627–10635, 2015.

[17] M. Tawfic and A. Hussein, "Multipurpose additive for ethylene propylene diene and acrylonitrile rubber blend," *Kautsch Gummi Kunstst (KGK)*, vol. 9, p. 30, 2015.

[18] H. E. Mayasari, A. Wirapraja, and I. Setyorini, "The blending of NBR/EPDM with montmorillonite as compatibilizer: the effect of different accelerator," *Majalah Kulit, Karet, dan Plastik*, vol. 36, no. 1, p. 1, 2020.

[19] S. M. R. Paran, G. Naderi, F. Javadi, R. Shemshadi, and M. R. Saeb, "Experimental and theoretical analyses on mechanical properties and stiffness of hybrid graphene/graphene oxide reinforced EPDM/NBR nanocomposites," *Materials Today Communications*, vol. 22, article 100763, 2020.

[20] S. Gunasekaran, R. K. Natarajan, A. Kala, and R. Jagannathan, "Dielectric studies of some rubber materials at microwave frequencies," *Indian Journal of Pure & Applied Physics (IJPAP)*, vol. 46, no. 10, p. 733.

[21] X. Zhao, K. Niu, Y. Xu et al., "Morphology and performance of NR/NBR/ENR ternary rubber composites," *Composites Part B: Engineering*, vol. 107, pp. 106–112, 2016.

[22] D. K. Das-Gupta and P. C. Scarpa, *In Handbook of Low and High Dielectric Constant Materials and Their Applications*, H. S. Nalwa, Ed., Academic Press, Burlington, 1999.

[23] S. P. Mahapatra, D. K. Tripathy, and Y. Lee, "Electrical response of microcellular EPDM rubber composites: complex dielectric modulus formalism and current–voltage characteristics," *Polymer Bulletin*, vol. 68, no. 7, pp. 1965–1976, 2012.

[24] S. K. Tiwari, R. N. P. Choudhary, and S. P. Mahapatra, "Relaxation behavior of chlorobutyl elastomer nanocomposites: effect of temperature, multiwalled carbon nanotube and frequency," *Journal of Polymer Research*, vol. 20, 2013.

[25] M. Razzaghi-Kashani, N. Gharavi, and S. Javadi, "The effect of organo-clay on the dielectric properties of silicone rubber," *Smart Materials and Structures*, vol. 17, no. 6, article 065035, 2008.

[26] W. Zepu, J. K. Nelson, M. Jianjun et al., "Effect of high aspect ratio filler on dielectric properties of polymer composites: a study on barium titanate fibers and graphene platelets," *IEEE Transactions on*, vol. 19, no. 3, pp. 960–967, 2012.

[27] O. A. Al-Hartomy, A. A. Al-Ghamdi, F. Al-Salamy et al., "Dielectric and microwave properties of graphene nanoplatelets/carbon black filled natural rubber composites," *International Journal of Materials and Chemistry*, vol. 2, no. 3, pp. 116–122, 2012.

[28] K. Ravikumar, K. Palanivelu, and K. Ravichandran, "Dielectric properties of natural rubber composites filled with graphite," *Materials Today: Proceedings*, vol. 16, pp. 1338–1343, 2019.

[29] V. Singh, D. Joung, L. Zhai, S. Das, S. I. Khondaker, and S. Seal, "Graphene based materials: past, present and future," *Progress in Materials Science*, vol. 56, no. 8, pp. 1178–1271, 2011.

[30] J. Qiu and S. Wang, "Enhancing polymer performance through graphene sheets," *Journal of Applied Polymer Science*, vol. 119, no. 6, pp. 3670–3674, 2011.

[31] K. S. Novoselov, A. K. Geim, S. V. Morozov et al., "Electric field effect in atomically thin carbon films," *Science*, vol. 306, no. 5696, pp. 666–669, 2004.

[32] Y. Srinivasarao, Y. Hanum, C. H. Chan, N. Kalarikkal, and T. Sabu, "Electrical properties of graphene filled natural rubber composites," *Advanced Materials Research*, vol. 812, pp. 263–266, 2013.

[33] C. S. Chandran, S. Yaragalla, N. Kalarikkal, R. Subban, C. H. Chan, and S. Thomas, "Effect of Reinforcement on the Barrier and Dielectric Properties of Epoxidized Natural Rubber–Graphene Nanocomposites," *Polymer Engineering And Science*, vol. 55, 2015.

[34] X. Duan, R. Tao, Y. Chen et al., "Improved mechanical, thermal conductivity and low heat build-up properties of natural rubber composites with nano-sulfur modified graphene oxide/silicon carbide," *Ceramics International*, vol. 48, pp. 22094–22104, 2022.

[35] B. Mensah, K. C. Gupta, H. Kim, W. Wang, K.-U. Jeong, and C. Nah, "Graphene-reinforced elastomeric nanocomposites: a review," *Polymer Testing*, vol. 68, pp. 160–184, 2018.

[36] S.-H. Bae, Y. Lee, B. K. Sharma, H.-J. Lee, J.-H. Kim, and J.-H. Ahn, "Graphene-based transparent strain sensor," *Carbon*, vol. 51, pp. 236–242, 2013.

[37] C. S. Boland, U. Khan, C. Backes et al., "Sensitive, high-strain, high-rate bodily motion sensors based on graphene–rubber composites," *ACS Nano*, vol. 8, no. 9, pp. 8819–8830, 2014.

[38] X. You and J. J. Pak, "Graphene-based field effect transistor enzymatic glucose biosensor using silk protein for enzyme immobilization and device substrate," *Sensors and Actuators B: Chemical*, vol. 202, pp. 1357–1365, 2014.

[39] T. Kuila, S. Bose, P. Khanra, A. K. Mishra, N. H. Kim, and J. H. Lee, "Recent advances in graphene-based biosensors," *Biosensors and Bioelectronics*, vol. 26, no. 12, pp. 4637–4648, 2011.

[40] T. T. Tung, R. Karunagaran, D. N. H. Tran et al., "Engineering of graphene/epoxy nanocomposites with improved distribution of graphene nanosheets for advanced piezo-resistive mechanical sensing," *Journal of Materials Chemistry C*, vol. 4, no. 16, pp. 3422–3430, 2016.

[41] W. Chen and L. Yan, "Preparation of graphene by a low-temperature thermal reduction at atmosphere pressure," *Nanoscale*, vol. 2, no. 4, pp. 559–563, 2010.

[42] H. Chen, Y. Xu, M. Liu, and T. Li, "An experimental study on the dielectric properties of rubber materials," *Polymers*, vol. 13, no. 17, p. 2908, 2021.

[43] B. Mensah, D. Kumar, D.-K. Lim, S. G. Kim, B.-H. Jeong, and C. Nah, "Preparation and properties of acrylonitrile–butadiene rubber–graphene nanocomposites," *Journal of Applied Polymer Science*, vol. 132, no. 36, 2015.

[44] B. Mensah, S. Kim, S. Arepalli, and C. Nah, "A Study of Graphene Oxide-Reinforced Rubber Nanocomposite," *Journal of Applied Polymer Science*, vol. 131, 2014.

[45] P. Blake, E. W. Hill, A. H. Castro Neto et al., *Applied Physics Letters*, vol. 91, 2007.

[46] M. Hernández, M. Bernal, R. Verdejo, T. A. Ezquerra, and M. A. López-Manchado, "Overall performance of natural rubber/graphene nanocomposites," *Composites Science and Technology*, vol. 73, pp. 40–46, 2012.

[47] X. Bai, C. Wan, Y. Zhang, and Y. Zhai, "Reinforcement of hydrogenated carboxylated nitrile–butadiene rubber with exfoliated graphene oxide," *Carbon*, vol. 49, no. 5, pp. 1608–1613, 2011.

[48] C. Li, C. Feng, Z. Peng, W. Gong, and L. Kong, "Ammonium-assisted green fabrication of graphene/natural rubber latex composite," *Polymer Composites*, vol. 34, no. 1, pp. 88–95, 2013.

[49] M. Vadivel, M. Suresh, M. S. Kumar, C. Vedhi, V. Selvam, and D. Raja, "Development and corrosion performance of 3- aminopropyltriethoxysilane grafted epoxidized ethylene-propylene-diene terpolymer rubber coatings," vol. 200, 2015.

[50] V. Jovanovic, J. Budinski-Simendic, S. Samardzija-Jovanovic, G. Markovic, and M. Marinovic-Cincovic, "The influence of carbon black on curing kinetics and thermal aging of acrylonitrile-butadiene rubber," *Chemical Industry & Chemical Engineering Quarterly*, vol. 15, no. 4, pp. 283–289, 2009.

[51] V. Jovanović, S. Samaržija-Jovanović, J. Budinski-Simendić, G. Marković, and M. Marinović-Cincović, "Composites based on carbon black reinforced NBR/EPDM rubber blends," *Composites Part B: Engineering*, vol. 45, no. 1, pp. 333–340, 2013.

[52] S. Samaržija-Jovanović, V. Jovanović, G. Marković, S. Konstantinović, and M. Marinović-Cincović, "Nanocomposites based on silica-reinforced ethylene–propylene–diene–monomer/acrylonitrile–butadiene rubber blends," *Composites Part B: Engineering*, vol. 42, no. 5, pp. 1244–1250, 2011.

[53] B. Mensah, K. C. Gupta, G. Kang, H. Lee, and C. Nah, "A comparative study on vulcanization behavior of acrylonitrile-butadiene rubber reinforced with graphene oxide and reduced graphene oxide as fillers," *Polymer Testing*, vol. 76, pp. 127–137, 2019.

[54] S. Gunasekaran, R. K. Natarajan, and A. Kala, "FTIR spectra and mechanical strength analysis of some selected rubber derivatives," *Spectrochimica Acta Part A: Molecular and Biomolecular Spectroscopy*, vol. 68, no. 2, pp. 323–330, 2007.

[55] B. Mensah, S. I. Kang, W. Wang, and C. Nah, "Effect of graphene on polar and nonpolar rubber matrices," *Mechanics of Advanced Materials and Modern Processes*, vol. 4, no. 1, p. 1, 2018.

[56] J. Wu, W. Xing, G. Huang et al., "Vulcanization kinetics of graphene/natural rubber nanocomposites," *Polymer*, vol. 54, no. 13, pp. 3314–3323, 2013.

[57] A. S. Sethulekshmi, J. S. Jayan, A. Saritha, and K. Joseph, "Recent developments in natural rubber nanocomposites containing graphene derivatives and its hybrids," *Industrial Crops and Products*, vol. 177, article 114529, 2022.

[58] M. A. Kader and C. Nah, "Influence of clay on the vulcanization kinetics of fluoroelastomer nanocomposites," *Polymer*, vol. 45, no. 7, pp. 2237–2247, 2004.

[59] S.-M. Kim and K.-J. Kim, "Effects of accelerators on the vulcanization properties of silica vs. carbon black filled natural rubber compounds," *Polymer Korea*, vol. 37, no. 3, pp. 269–275, 2013.

[60] S.-S. Choi, "Effect of bound rubber on characteristics of highly filled styrene-butadiene rubber compounds with different types of carbon black," *Journal of Applied Polymer Science*, vol. 93, no. 3, pp. 1001–1006, 2004.

[61] J. Fröhlich, W. Niedermeier, and H. D. Luginsland, "The effect of filler–filler and filler–elastomer interaction on rubber reinforcement," *Composites Part A: Applied Science and Manufacturing*, vol. 36, no. 4, pp. 449–460, 2005.

[62] J. Wilk, R. Smusz, R. Filip, G. Chmiel, and T. Bednarczyk, "Experimental investigations on graphene oxide/rubber composite thermal conductivity," *Scientific reports*, vol. 10, Article ID 15533, 2020.

[63] B. Mensah, D. Kumar, D. K. Lim, S. Kim, B. H. Jeong, and C. Nah, "Electrode polarization vs. Maxwell-Wagner-Sillars interfacial polarization in dielectric spectra of materials: Characteristic frequencies and scaling laws," *Journal of Applied Polymer Science*, vol. 132, 2015.

[64] M. Samet, V. Levchenko, G. Boiteux, G. Seytre, A. Kallel, and A. Serghei, "Electrode polarization vs. Maxwell-Wagner-Sillars interfacial polarization in dielectric spectra of materials: characteristic frequencies and scaling laws," *The Journal of Chemical Physics*, vol. 142, no. 19, article 194703, 2015.

[65] A. Serghei, M. Tress, J. R. Sangoro, and F. Kremer, "Electrode polarization and charge transport at solid interfaces," *Physical Review B*, vol. 80, no. 18, article 184301, 2009.

[66] P. Barber, S. Balasubramanian, Y. Anguchamy et al., "Polymer composite and nanocomposite dielectric materials for pulse power energy storage," *Materials*, vol. 2, pp. 1697–1733, 2009.

[67] L. Pinchuk, B. Jurkowski, B. Jurkowska, A. Kravtsov, and V. Goldade, "On some variations in rubber charge state during processing," *European Polymer Journal*, vol. 37, no. 11, pp. 2239–2243, 2001.

[68] Z. Wang, J. K. Nelson, H. Hillborg, S. Zhao, and L. S. Schadler, "Electrical insulation and dielectric phenomena (CEIDP)," in *2012 Annual Report Conference on, 14-17 Oct. 2012*, p. 40, Quebec, QC, Canada, 2012.

[69] T. T. N. Dang, S. P. Mahapatra, V. Sridhar, J. K. Kim, K. J. Kim, and H. Kwak, "Dielectric properties of nanotube reinforced butyl elastomer composites," *Journal of Applied Polymer Science*, vol. 113, no. 3, pp. 1690–1700, 2009.

[70] I. Tantis, G. C. Psarras, and D. Tasis, "Functionalized graphene – poly(vinyl alcohol) nanocomposites: physical and dielectric properties," *Express Polymer Letters*, vol. 6, no. 4, pp. 283–292, 2012.

[71] L. E. Sutton, "Dielectric behavior and structure. Dielectric constant and loss, dipole moment and molecular structure," *Journal of the American Chemical Society*, vol. 78, no. 2, pp. 507-508, 1956.

[72] M. Akram, A. Javed, and T. Z. Rizvi, "Dielectric properties of industrial polymer composite materials," *Turkish Journal of Physics*, vol. 29, p. 355, 2005.

[73] Z. M. Dang, L. Wang, Y. Yin, Q. Zhang, and Q. Q. Lei, "Giant dielectric permittivities in functionalized carbon-nanotube/electroactive-polymer nanocomposites," *Advanced Materials*, vol. 19, no. 6, pp. 852–857, 2007.

[74] F. He, S. Lau, H. L. Chan, and J. T. Fan, "High dielectric permittivity and low percolation threshold in nanocomposites based on poly(vinylidene fluoride) and exfoliated graphite nanoplates," *Advanced Materials*, vol. 21, no. 6, pp. 710–715, 2009.

[75] H. Nalwa, *Handbook of Low and High Dielectric Constant Materials and Their Applications*, Academic Press, London, 1999.

[76] P. N. Kumta and J. Yong Kim, *In Handbook of Low and High Dielectric Constant Materials and Their Applications*, H. S. Nalwa, Ed., Academic Press, Burlington, 1999.

[77] I. M. Hodge, M. D. Ingram, and A. R. West, "Impedance and modulus spectroscopy of polycrystalline solid electrolytes," *Journal of Electroanalytical Chemistry and Interfacial Electrochemistry*, vol. 74, no. 2, pp. 125–143, 1976.

[78] F. Tian and Y. Ohki, "Electric modulus powerful tool for analyzing dielectric behavior," *IEEE Transactions on Dielectrics and Electrical Insulation*, vol. 21, no. 3, pp. 929–931, 2014.

[79] N. McCrum, B. E. Read, and G. Williams, *Anelastic and Dielectric Effects in Polymeric Solids*, John Wiley & Son, 1967.

[80] R. Richert and H. Wagner, "The dielectric modulus: relaxation versus retardation," *Solid State Ionics*, vol. 105, no. 1-4, pp. 167–173, 1998.